Che *et al. Chem Synth* 2024;4:64
**DOI:** 10.20517/cs.2024.62

**Chemical Synthesis**

**Research Article**

**Open Access**

Check for updates

# Efficient selective hydrogenation of phenylacetylene over Pd-based rare earth dual-atomic catalysts

**Leisheng Che[1,#], Ziyun Zhong[1,#], Peng Cui[2], Yaping Du[1,*], Hongbo Zhang[1,*]**

[1]School of Materials Science and Engineering, Tianjin Key Laboratory for Rare Earth Materials and Applications, Haihe Laboratory of Sustainable Chemical Transformation, Nankai University, Tianjin 300350, China
[2]Key Laboratory of Functionalized Molecular Solids, Ministry of Education, Anhui Laboratory of Molecule-based Materials, College of Chemistry and Materials Science, Anhui Normal University, Wuhu 241002, Anhui, China.
[#]Authors contributed equally.

[*]**Correspondence to:** Prof. Hongbo Zhang, Prof. Yaping Du, School of Materials Science and Engineering, Tianjin Key Laboratory for Rare Earth Materials and Applications, Haihe Laboratory of Sustainable Chemical Transformation, Nankai University, No.38 Tongyan Road, Jinnan District, Tianjin 300350, China. hbzhang@nankai.edu.cn; ypdu@nankai.edu.cn

**How to cite this article:** Che L, Zhong Z, Cui P, Du Y, Zhang H. Efficient selective hydrogenation of phenylacetylene over Pd-based rare earth dual-atomic catalysts. *Chem Synth* 2024;4:64. https://dx.doi.org/10.20517/cs.2024.62

**Received:** 19 May 2024 **First Decision:** 25 Jul 2024 **Revised:** 26 Aug 2024 **Accepted:** 18 Sep 2024 **Published:** 17 Oct 2024

**Academic Editor:** Ying Wan **Copy Editor:** Pei-Yun Wang **Production Editor:** Pei-Yun Wang

## Abstract

Selective hydrogenation of phenylacetylene to styrene plays a vital role in fine chemical synthesis with palladium (Pd)-based catalysts as the active components and usually suffered from low selectivity due to over-hydrogenation and low stability through polymerization (c.a. green oil generation). In this work, we found that by confining the Pd atom within a Pd-Ln (Ln: rare earth elements, such as Y, Lu, *etc.*) diatomic structure [diatomic catalyst (DAC)], the reaction performance of selective hydrogenation of phenylacetylene has been greatly promoted, in which 92% styrene selectivity has been determined at 100% phenylacetylene conversion. This would be attributed to the diatomic structure established, which was achieved by introducing Pd-Ln precursors and confirmed by high-angle annular dark-field scanning transmission electron microscopy (HAADF-STEM) and X-ray adsorption fine structure (XAFS) characterizations and it was demonstrated that slight electron transfer from Ln to the adjacent isolated Pd makes it slightly negatively charged and facilitated the styrene formation. Besides, a Langmuir-Hinshelwood model was established to describe the whole reaction mechanism. After a systematic kinetic investigation, it suggests that the $C_8H_6^*$ + $H^*$ elementary step is probably the kinetically relevant for the whole reaction and the surface of the catalyst is mainly covered by $C_8H_6^*$. The energy relationship of each step along phenylacetylene hydrogenation was quantitatively described by means of parity fitting and gas isothermal adsorption, providing insights into the selective hydrogenation of phenylacetylene over 0.02%Pd-Ln/C (Ln = Y/Lu) catalysts and pave the way of catalytic design at the atomic level.

**Keywords:** Rare earth elements, phenylacetylene hydrogenation, diatomic catalyst, reaction mechanism

## INTRODUCTION

Styrene has extensive applications in industrial feedstock generations such as rubber, medicine, pesticides and pigments[1,2]. Typically, it is extracted from the cracked oil[3]. Within this process, as a toxic compound in the styrene ingredients, the amount of phenylacetylene should be controlled below 10 ppm; otherwise, it will be gradually enriched in the styrene extraction process, resulting in poisoning against the subsequent process of styrene polymerization[3,4]. Thus, the selective hydrogenation of phenylacetylene to styrene is a very important step before styrene utilization[5,6]. Nevertheless, as phenylacetylene might be over-hydrogenated, an undesired byproduct ethylbenzene is inevitably produced. Hence, it is urgent to develop phenylacetylene semi-hydrogenation catalysts with both high selectivity and activity.

Owing to their outstanding catalytic performance and good application prospects, various heterogeneous metal catalysts have been widely applied in the selective hydrogenation of alkynes [Supplementary Table 1][7,8]. Among them, palladium (Pd)-based catalysts have attracted great attention due to their superior overall intrinsic activity[9,10]. We summarized the results of phenylacetylene hydrogenation performance and catalytic stability of Pd-based catalysts in phenylacetylene hydrogenation in the literature [Supplementary Tables 2 and 3]. Unfortunately, unmodified Pd catalysts have low selectivity to olefines due to severe side reactions of excessive hydrogenation, which is mainly owing to the formation of β-hydride (β-H) species on the subsurface of the Pd nanoparticles or clusters that are more active than those adsorbed surface hydrogen species[9]. For modified Pd-based catalysts, such as commercial Pd-Ag catalysts, they exhibit high activity and selectivity in the selective hydrogenation of alkynes[11]. However, due to the formation of green oil and coke on the surface of the catalyst, the stability is insufficient[8]. Accordingly, the "active site isolation" strategy had been developed to improve the stability by reducing the amount of adsorbed surface species that caused severe oligomerization (i.e., formation of green oil) and coking[8,12,13]. Surface modification, such as the addition of a second toxic metal (Pb, Sn, *etc.*) or organic reagents, is a common strategy to improve the overall reaction performance[14,15]. However, selectivity is usually improved by sacrificing reactivity, where a large percentage of the active sites was covered and inaccessible[8,16,17]. Increasing the surface atomic ratio of metal active sites in catalysts is an effective strategy for improving catalytic performance[18]. For example, reducing the size of metal particles and increasing metal dispersion can effectively increase the exposed metal active sites on the surface. Correspondingly, atomically dispersed materials (ADMs) have been developed by researchers. ADMs can maximize atomic efficiency, increase reactive sites, and reduce metal loss, and have been widely applied in different fields[19]. For example, Zhu *et al.* designed a p-block-element Bi-based catalysts made up of atomically dispersed Bi and Bi nanoclusters for highly selective electrocatalytic $2e^-$ oxygen reduction reaction (ORR)[20]. Zhao *et al.* utilized the high reducing ability and suitable surface defects of MXene ($Ti_3C_2$) to prepare atomically dispersed Pt single-atom catalysts (SACs) ($Pt_1/Ti_{3-x}C_2T_y$) by self reduction method, demonstrating excellent catalytic performance in the formylation reaction of amines in carbon dioxide[21]. Recently, SACs, as a type of ADMs, have emerged as a new frontier in heterogeneous catalysis owing to their maximum atomic utilization nature and unique coordinately unsaturated sites preserved[22-26]. For instance, the $Pd_1$/Ni@G SAC synthesized by Zhao *et al.* achieved 93% selectivity in styrene formation under complete conversion of phenylacetylene under mild conditions[3]. Similarly, the $Pd_1/TiO_2$ SAC prepared by Liu *et al.* can simultaneously achieve 99% conversion of phenylacetylene and 91% selectivity of styrene at room temperature[27]. Although SACs show good potential in selective hydrogenation of alkynes[28-30], they still suffer from low metal loadings, aggregation issues and poor stability[31]. It has been reported that due to the synergistic effect between the bimetals, the electronic structure and geometric structure of the active sites of the bimetallic Pd-based catalysts could be modified with great flexibility compared with monometallic Pd catalysts, providing more possibilities for improving the catalytic performance[32-34]. The adjusted electronic

structure could alter the adsorption configuration and strength of the reaction intermediates and regulate the catalytic reaction performance[35]. Changes in local chemical adsorption properties are on account of the arrangement of local atoms at the adsorption site, such as the adsorption configuration of reactant/product molecules, which could also regulate the adsorption intensity, thereby affecting the catalytic performance[36]. Compared with SACs, the diatomic catalysts (DACs) made from adjacent two isolated sites possess higher metal loadings, more complex and adjustable active sites, and potential synergistic effects between bimetals, providing more opportunities to achieve better catalytic performance[31-38]. It has been reported that alkyne hydrogenation can be improved by introducing a second metal to construct a diatomic structure and utilizing the synergistic effect between diatomic sites. For instance, the Pd-Ru@ZIF-8 bimetallic site catalyst synthesized by Li *et al.* obtained 98% phenylacetylene conversion and 96% styrene selectivity[38]. The problem relies on complexity of establishing this DAC system, especially on material preparations, compared with the SACs.

Rare earth elements, known as industrial vitamins, are extensively applied as dopants to enhance catalytic performance, so that the catalysts in the target reactions have excellent selectivity, reactivity and durability[39-41]. Rare earth elements have a unique electronic configuration, which give an additional rhythm to adjust their functional properties from the perspective of electronic modification, and have a significant prospect in improving the materials activity and stability[40]. Currently, DACs containing rare earth elements and noble metals are rarely studied in thermal catalytic reactions while being more often applied in electrocatalysis[42-47]. Therefore, this combination results in a new strategy in selective hydrogenation of phenylacetylene and will pave the way in catalytic design at atomic level.

In this work, we develop a Pd-based rare earth DAC for the selective hydrogenation of phenylacetylene in the gas phase, denoted as Pd-Ln/C (Ln = Y/Lu), the structure of which was confirmed by high-angle annular dark-field scanning transmission electron microscopy (HAADF-STEM) and X-ray adsorption fine structure (XAFS) characterizations. Under reaction conditions (0.3 kPa $C_8H_6$, 30 kPa $H_2$, balance with Ar, 393 K), robust and optimized catalytic performance was achieved for the selective hydrogenation of phenylacetylene, in which the selectivity of styrene at complete conversion of phenylacetylene was determined at 92%. And systematic kinetic studies showed that 0.02%Pd-Y/C and 0.02%Pd-Lu/C probably experience the same rate-determining step (RDS) of "$C_8H_6^*$ + $H^*$" and both are primarily covered by $C_8H_6^*$ [most abundant surface intermediates (MASIs)]. Meanwhile, combined with the thermodynamic and kinetic parameters acquired by parity fittings and isotherm gas adsorption experiments, the energy changes of the transition state of phenylacetylene hydrogenation were quantitatively described, and the entire reaction process was systematically described, which exhibits a good complement to the theoretical results in the literature.

## EXPERIMENTAL

### Synthesis of Pd-Ln (Ln = Y/Lu) precursor

The single-source precursors (SSPs) used for the synthesis of DACs were prepared according to the literature[48]. Whole synthesis operations were carried out under inert gas protected by nitrogen with a standard Schlenk-line and glovebox. In a typical synthesis process, complex I (0.2 g, 0.29 mmol) was dissolved in 2 mL of methylbenzene. Then, the solution was carefully added to another solution containing the ligand ($Ph_2PCH_2NHPh$) (0.169 g, 0.58 mmol) in 2 mL methylbenzene at room temperature under continuous stirring for 1.5 h. And the bright yellow aqua solution was filtrated and layered with 5 mL hexane at room temperature to yield the complex II as pale yellow crystals. Complex II (0.2 g, 0.20 mmol) dispersed in 2 mL methylbenzene was step-wisely added to a solution of $(COD)Pd(CH_2SiMe_3)_2$ prepared following the reported procedure[49] (0.078 g, 0.20 mmol) in toluene (2 mL) at room temperature under

stirring for 2 h. And the bright yellow solution was filtrated and layered with 5 mL of hexane to yield SSPs as light-yellow crystals, too, which is the SSP received.

### Synthesis of Pd-Ln/C (Ln = Y/Lu) catalysts

In the glovebox, 5 mg SSP was dissolved in 10 mL anhydrous toluene and the orange solution was kept in the refrigerator. In a typical synthesis procedure, the quantitative amount of the solution was added into the anhydrous toluene solution containing 100 mg of carbon support (Ketjen Black EC600J) under stirring. After stirring for 2 h, the toluene within the dispersion was removed in vacuum. The mixture was then transferred to a quartz boat and introduced into a tube furnace from the glovebox quickly. Before the heat treatment, air was removed from the tube furnace by introducing 10% $H_2$/Ar (200 mL/min) gas mixtures. The tube furnace temperature was raised from room temperature to 473 K at the ramp of 10 K/min and held at this temperature for 2 h prior to cooling down to the room temperature. The sample acquired was denoted as 0.02%Pd-Y/C. By altering the amounts of SSP, we prepared the X%Pd-Y/C catalysts, in which X denotes the mass of Pd (X = 0.02, 0.05, 0.1, 0.5 and 1). Meanwhile, Pd-Lu/C catalysts were prepared following similar procedures.

### Catalytic performance evaluation

Performance evaluation of phenylacetylene hydrogenation at atmospheric pressure was conducted in a packed-bed glass pipe reactor with 6 mm internal diameter. The temperature of the catalyst bed was monitored by a proportional-integral-differential (PID) controller provided with a K-type thermocouple, which was in direct contact with the catalyst bed. Prior to the evaluation of the catalytic performance, 20 mg catalyst was evenly mixed with silica (99%, Sigma-Aldrich) and pre-reduced for 1 h in 10 % $H_2$/Ar (50 mL/min) at 473 K, and then the system was purged with Ar (50 mL/min) at identical temperature. The overall pressure of the reaction system was fixed at 1 atm and balanced with Ar. In a 10 mL liquid syringe, 1 mL of phenylacetylene ($C_8H_6$, Macklin, 98%) was introduced as the reactant and mixed with 9 mL of cyclohexane ($C_6H_{12}$, Energy Chemical, 99.5%) as the solvent. The catalyst was stabilized under a typical reaction condition [30 kPa $H_2$, 0.3 kPa $C_8H_6$, 2.784 kPa $C_6H_{12}$, balance with Ar, weight hourly space velocity (WHSV) = 63.6 $h^{-1}$] before any catalytic test. The generated products were qualitatively and quantitatively calibrated by gas chromatography (SCION, 436-GC) equipped with a capillary column (HP Al S) and flame ion detector (FID). After ten hours of stability test, phenylacetylene conversion, styrene and ethylbenzene selectivity, and the hydrogenation rate were estimated in accordance with the formula below by analyzing the peak areas and factors of the reactants and products calibrated by gas chromatography:

$$C_8H_6 \text{ conversion } (\%) = \left( \frac{[C_8H_6]_{inlet} - [C_8H_6]_{outlet}}{[C_8H_6]_{inlet}} \right) \times 100\% \quad (1)$$

$$C_8H_8 \text{ selectivity } (\%) = \left( 1 - \frac{[C_8H_{10}]_{outlet}}{[C_8H_6]_{inlet}} \right) \times 100\% \quad (2)$$

$$C_8H_{10} \text{ selectivity } (\%) = \left( 1 - \frac{[C_8H_8]_{outlet}}{[C_8H_6]_{inlet}} \right) \times 100\% \quad (3)$$

$$TOR = \frac{\text{Mole of } C_8H_6 \text{ converted per min}}{[Pd]} \quad (4)$$

where $[C_8H_6]_{inlet}$ and $[C_8H_6]_{outlet}$ denote the concentrations of phenylacetylene at the inlet and outlet, respectively. $[C_8H_8]_{outlet}$ and $[C_8H_{10}]_{outlet}$ indicate the concentrations of styrene and ethylbenzene at the outlet.

Moreover, [Pd] represents the quality of metal Pd in the catalyst.

## RESULTS AND DISCUSSION

### Catalyst characterizations

We have conducted various characterizations against the as-prepared catalysts, and the concrete characterization methods can be found in the Supplementary Materials (as shown in the Experimental procedure 1.1-1.4). Supplementary Figure 1 displays the sketch map of the synthesis of Pd-Y/C catalysts with diverse Pd loadings, in which the synthesized Pd-Y SSP and carbon powder were dispersed in anhydrous toluene and stirred for 2 h, after which the toluene solution was removed and the resulting sample was placed in a tube furnace for 2 h in a flowing 10%$H_2$/Ar mixture at 473 K to obtain the Pd-Y/C catalyst. Supplementary Figure 2 displays the X-ray diffraction (XRD) patterns of the 0.02%Pd-Ln/C (Ln = Y/Lu) DACs, in which characteristic peaks of carbon support were selectively identified within the XRD patterns of 0.02%Pd-Ln/C (Ln = Y/Lu) DACs while the signal of Pd was almost invisible owing to the low content of metallic Pd in the catalyst. The Pd and Y distributions in 0.02%Pd-Y/C DAC were examined by the HAADF-STEM as displayed in Figure 1A and B. As shown by the yellow ovals in Figure 1A and C, the concentrated distribution separated bright points represent the Pd and Y atoms. In addition to the isolated single-atom centers and small clusters that could be assigned to Pd (or Y) single-atoms and Pd-Y small clusters, separately, abundant adjacent metal atoms or Pd-Y diatomic sites were determined. In current articles on diatomic or SACs, many scholars have used signal strength to characterize the existence of diatomic or single-atom structures. The Pd-Y bonding of the diatomic pairs was statistically analyzed and showed a distance of 0.24 ± 0.03 nm [Figure 1D], which approaches the distance of Pd and Y (~0.286 nm)[48] from the precursor as described in Supplementary Figure 3, indicating that the precursor was probably preserved. Since the difference in Z-contrast between Pd or Y and the carbon support, the intensity distribution of the labeled sites in Figure 1E suggests the presence of contiguous Pd-Y atomic pairs. The result of energy dispersive X-ray spectroscopy (EDS) revealed the coexistence of highly dispersed Pd and Y atoms anchored to the surface of carbon support [Figure 1B]. Therefore, the results observed under an electron microscope reveal the coexistence of Pd-Y diatomic species, Pd (or Y) single-atom species and small Pd-Y clusters.

The existence of multi-structures of surface species was further confirmed by XAFS spectroscopy as described in Figure 2, in which both the chemical state and the coordination environments of Pd and Y within Pd-Y/C DACs and Pd within Pd/C SACs have been probed. It is worth noting that the 0.5%Pd-Y/C catalyst and 0.5%Pd/C were selected for XAFS analysis due to limited content of Pd and Y elements in the 0.02%Pd-Y/C and 0.02%Pd/C samples that caused undetectable signals during X-ray analysis. Specifically, Figure 2A displayed the X-ray adsorption near-edge structure (XANES) spectra at the Pd K-edge for 0.5%Pd-Y/C, 0.5%Pd/C and the reference Pd foil and PdO samples. The peak position of white lines of 0.5%Pd-Y/C is close to that of the Pd foil and the adsorption profile near the edge is slightly greater than that of the Pd foil, demonstrating that the Pd species in 0.5%Pd-Y/C exhibited similar electronic state compared to metallic Pd and was slightly negatively charged. Figure 2B showed the extended X-ray absorption fine structure (EXAFS) oscillations in the R space for 0.5%Pd-Y/C, 0.5%Pd/C and reference samples. Similarly, as displayed in Figure 2C, the limited white line intensity of the Y K-edge indicated that the Y species in 0.5%Pd-Y/C has close to 0 valence states. Thus, probably the complex structure [Scheme 1] has been preserved or partially preserved during catalyst preparation; otherwise, Y should be more tentatively oxidized as reported in the literature[49-51]. There is probably an electronic interaction between Pd and Y in 0.5%Pd-Y/C, where the electron should shift from Y to Pd atoms since Pd is slightly negatively charged compared with Pd foil, and that is abnormal since this sample has already been exposed to the open air before XAFS analysis and the finely dispersed transition metal usually shows partially oxidized identity[52,53]. In addition, it has been reported that the binding of rare earth elements with transition

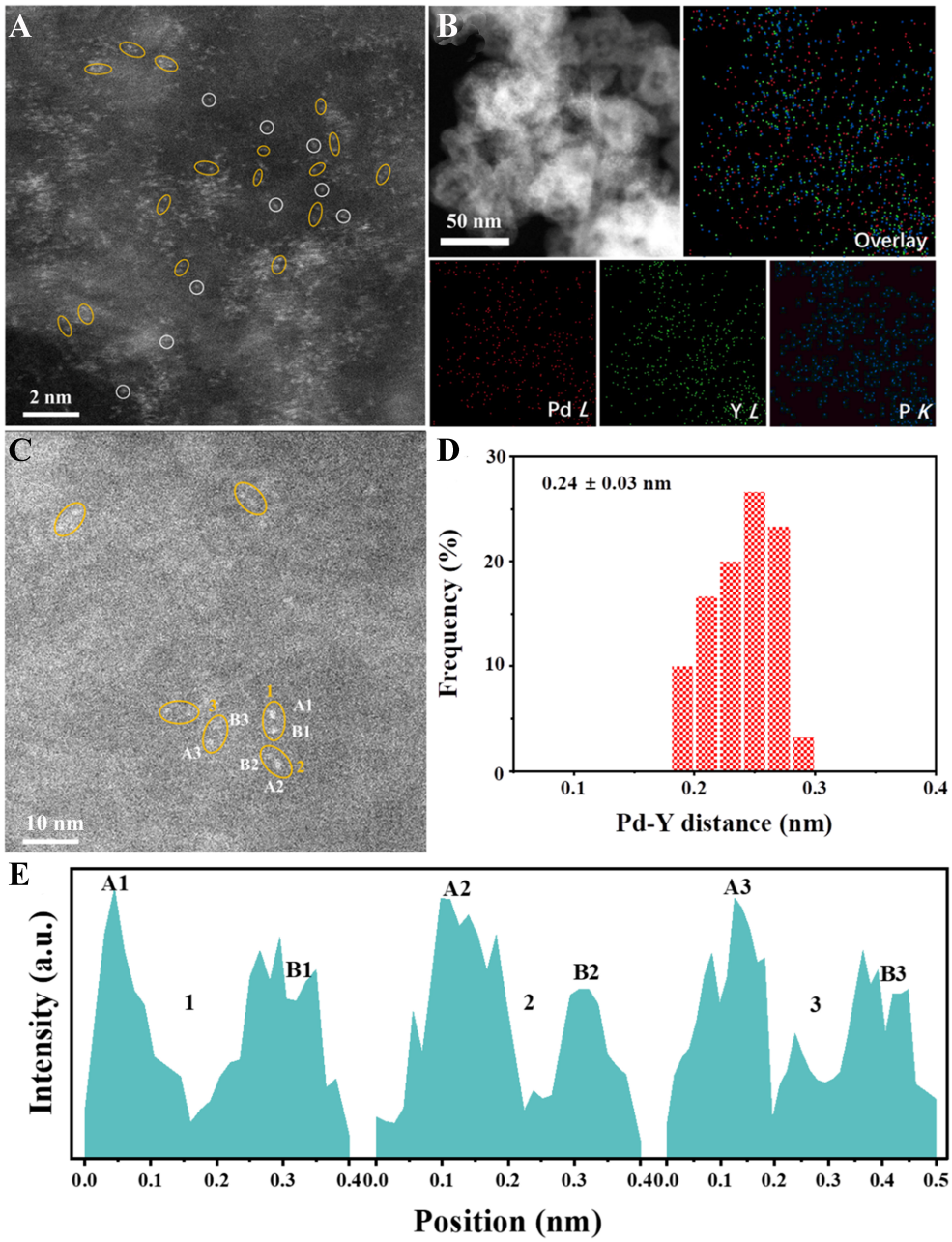


**Figure 1.** The characterizations of 0.02%Pd-Y/C. (A) Aberration-corrected HAADF-STEM images of 0.02%Pd-Y/C DAC (Pd-Y diatomic structures are emphasized by the yellow ovals, and Pd or Y single-atoms are marked with white circles); (B) TEM image and the EDS mappings of 0.02%Pd-Y/C DAC; (C) enlarged images of Pd-Y diatomic pairs; (D) statistical Pd-Y distance in the observed diatomic pairs; and (E) intensity distribution of ovals 1, 2, and 3 in image (C). HAADF-STEM: High-angle annular dark-field scanning transmission electron microscopy; DAC: diatomic catalyst; TEM: transmission electron microscopy; EDS: energy dispersive X-ray spectroscopy.

elements could induce charge transfer from the rare earth element to the transition metal leading to negatively charged chemical states[54]. All these findings could be further supported by the adsorption edges identified within the insert images of Figure 2A and C. In the Pd K-edge EXAFS spectra [Figure 2B], for 0.5%Pd-Y/C, two distinct peaks were identified at about 1.63 and 2.54 Å, close to the Pd–O bond (1.51 Å) of PdO and the Pd–Pd bond (2.55 Å) of Pd foil, respectively. It is also hard to distinguish the scattering of Pd-C

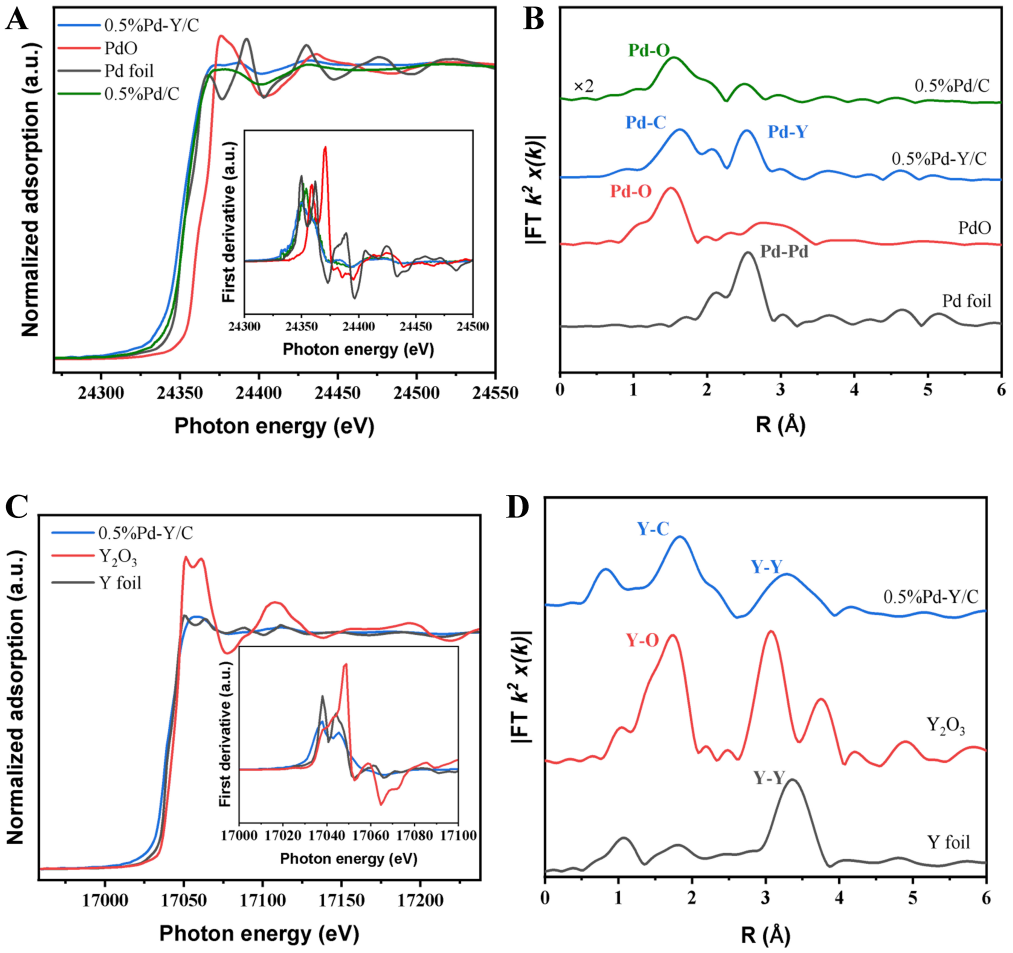


**Figure 2.** The XAFS spectroscopy of Pd-Y/C catalyst. (A) Normalized XANES profiles for the 0.5%Pd-Y/C, 0.5%Pd/C and reference samples at the Pd K-edge; Insert image is the first derivatives of the Pd XANES spectra; (B) EXAFS spectra of the Fourier transformed $k^2$-weighted χ(k) data for 0.5%Pd-Y/C, 0.5%Pd/C and references at the Pd K-edge; (C) Normalized XANES profiles for the 0.5%Pd-Y/C catalyst and reference samples at the Y K-edge; Insert image is the first derivatives of the Y XANES spectra; (D) EXAFS spectra of the Fourier transformed $k^2$-weighted χ(k) data for 0.5%Pd-Y/C catalyst and references at the Y K-edge. XAFS: X-ray adsorption fine structure; XANES: X-ray adsorption near-edge structure; EXAFS: extended X-ray absorption fine structure.

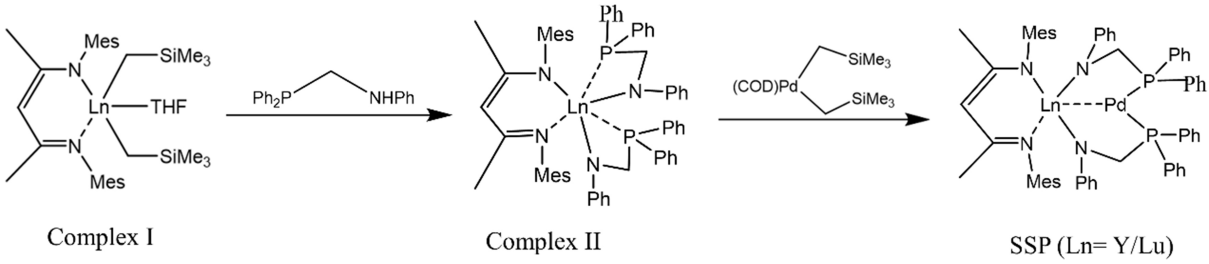


**Scheme 1.** Synthesis method of Pd-Ln (Ln = Y/Lu) SSP. SSP: Single-source precursor.

from Pd-P, Pd-N, Pd-O, *etc.* Nevertheless, due to the adsorption edge of Pd-Y DACs determined, the probed Pd is probably at a reducible chemical state and probably the first coordinated shell lies in a reducible environment; thus, Pd-C is more reasonable than any other possibilities considered. And the second shell was attributed to the Pd-Y scattering since negligible Pd clusters were determined by

transmission electron microscopy (TEM) analysis. Significant Pd-Pd scattering would not be prominent within this sample; thus, Pd-Y was assigned for the second peak in Figure 2B. In addition, according to the HAADF-STEM of 0.02%Pd-Y/C, the statistical average distance of Pd–Y bond was 2.4 Å, while the theoretical bond distance of Pd-Y in SSP is 2.86 Å[48]; thus, the peak located at 2.54 Å would be attributed to Pd-Y. For 0.5%Pd/C, only one obvious characteristic peak was identified at about 1.53 Å, close to the Pd–O bond (1.51 Å) of PdO, and no obvious characteristic peak of Pd–Pd bond was identified, indicating that 0.5%Pd/C was in single-atom coordination environment, which also suggested that 0.02%Pd/C catalyst might also be in a single-atomic state. As displayed in Figure 2D, the Fourier-transformed (FT)-EXAFS analysis of 0.5%Pd-Y/C revealed a predominated peak at around 1.83 Å, close to the Y–O bond (~1.73 Å) of $Y_2O_3$. However, the valence state of Y in 0.5%Pd-Y/C is mainly ~0; thus, the peak located at 1.83 Å was assigned to the scattering of the Y-C path[50,51]. In addition, compared with the Y foil, the Y–Y bond with the dominant peak located at 3.29 Å was also detected in the 0.5%Pd-Y/C catalyst, indicating that the Y species was dispersed on the carbon matrix with a Y-C and Y-Y coordination and suffered from slightly sintering. In addition, the HAADF-STEM results of the 0.5%Pd-Y/C catalyst [Supplementary Figure 4] indicate that it is mainly composed of Pd-Y diatomic pairs and Pd-Y clusters. In a word, the XANES and EXAFS profiles probed the geometric structure and electronic structure of 0.5%Pd-Y/C catalyst. Clearly, the 0.5%Pd-Y/C catalyst mainly consists highly dispersed Pd-Y active components with well reduced Pd-Y pairs confined by the carbon support. Probably, there are mild electronic donations from the Y to the adjacent Pd. Small amounts of agglomerated structures were also determined.

### Catalytic performance evaluation

To investigate the catalytic performance of Pd-based rare earth DACs in the selective hydrogenation of phenylacetylene in gas phase, we first compared the catalytic hydrogenation results obtained with different heat treatment temperatures and Pd loadings of the Pd-Y/C catalysts under the same reaction conditions. As displayed in Supplementary Figure 5A, for the 1%Pd-Y/C catalyst, the phenylacetylene conversion gradually increased with reaction temperature as the catalyst heat treatment temperature increased (from 723 to 923 K), while the selectivity of the main product styrene decreased and that of the by-product ethylbenzene increased rapidly [Supplementary Figure 5B and C]. We also considered the catalytic performance of Pd-Lu/C catalysts with various Pd loadings in the selective hydrogenation of phenylacetylene [Supplementary Figure 5D-F]. For the Pd-Lu/C catalysts, when the metal Pd loadings are higher than 0.1%, the full conversion of phenylacetylene can be achieved in the reaction temperature range of 393-473 K. However, the selectivity of styrene decreased from 77% to 1% with rising reaction temperature, and the selectivity of ethylbenzene as a by-product increased. For the 0.02%Pd-Lu/C catalyst, the conversion of phenylacetylene grew from 22% to 100% with the reaction temperature, and the selectivity of styrene reached the maximum of 93% at 393 K. Based on the TEM images and EDS mapping [Supplementary Figure 6A-D], it was known that there is significant amount of metal nanoparticles formed when the catalyst was heated to 923 K before the catalytic test compared with the sample treated at 723 K. It was reported that the subsurface of Pd nanoparticles is prone to facilitate the formation of β-H species leading to the over-hydrogenation of phenylacetylene[9]. After fixing the heat treatment temperature of the catalyst at 473 K and decreasing the loading of metal Pd, the styrene selectivity of 0.5%Pd-Y/C decreased from 86% to 2% as the reaction temperature increased from 333 to 473 K. In addition, with the increase of reaction temperature, the styrene selectivity of 0.1%Pd-Y/C decreased from 90% to 10%, and that of 0.05%Pd-Y/C decreased from 93% to 79%. In contrast, for the 0.02%Pd-Y/C catalyst, the styrene selectivity was constantly maintained at around 92% within the reaction temperature range applied. To better understand the influence of the heat treatment against the catalyst and metal Pd loading on styrene selectivity, we compared the styrene selectivity of a series of Pd-Y/C catalysts at fully phenylacetylene conversion (c.a. ~100% conv.) at 393 K, as displayed in Figure 3A. The selectivity to styrene increases with decreasing catalyst heat treatment temperature and metal Pd loading.

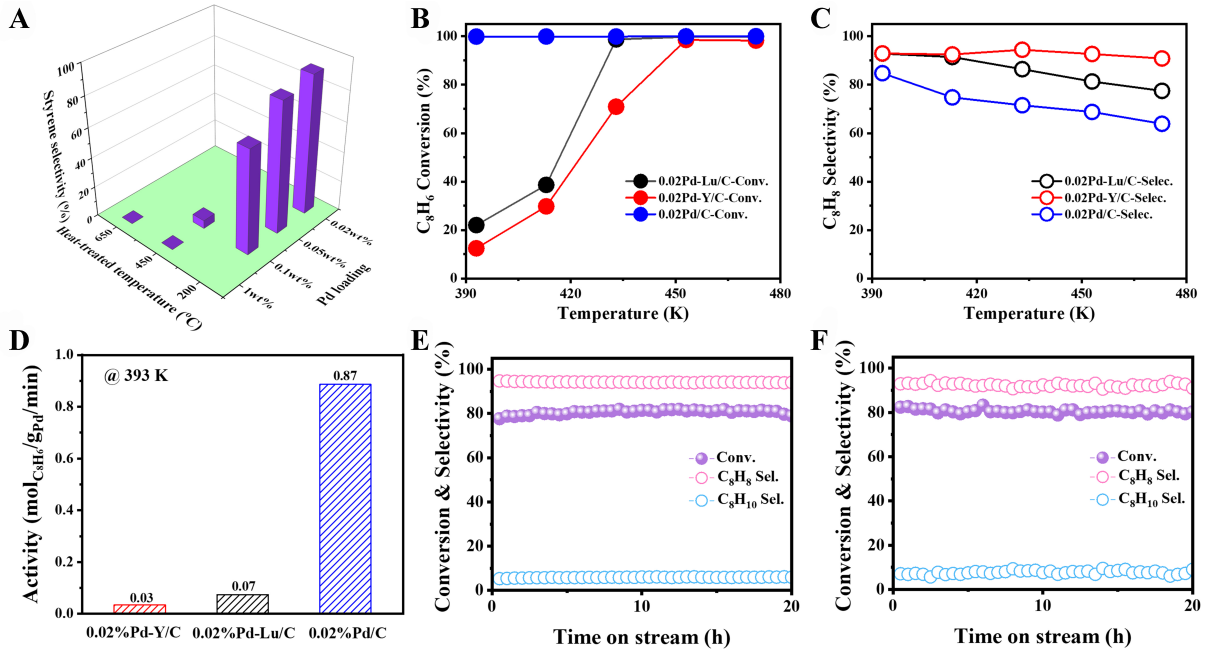


**Figure 3.** Catalytic performance evaluation. (A) Styrene selectivity comparison as a function of heat-treated temperature and Pd loadings at ~100% phenylacetylene conversion for selective hydrogenation of phenylacetylene over Pd-Y/C catalysts. Reaction conditions: 30 kPa $H_2$, 0.3 kPa $C_8H_6$, 2.784 kPa $C_6H_{12}$, balance with Ar, 393 K. Catalytic performance of 0.02%Pd/C SAC and 0.02%Pd-Ln/C (Ln = Y/Lu) DACs in selective hydrogenation of phenylacetylene: Phenylacetylene conversion (B) and styrene selectivity (C) as a function of reaction temperature; (D) Activity of these three samples at 393 K. Reaction condition: 30 kPa $H_2$, 0.3 kPa $C_8H_6$, 2.784 kPa $C_6H_{12}$, balance with Ar, 393-473 K, WHSV = 63.6 $h^{-1}$; (E) Durability test on 0.02%Pd-Y/C and (F) Durability test on 0.02%Pd-Lu/C in the selective hydrogenation of phenylacetylene for 20 h at 393 K. Reaction conditions: 30 kPa $H_2$, 0.3 kPa $C_8H_6$, 2.784 kPa $C_6H_{12}$, balance with Ar, WHSV = 25.4 $h^{-1}$. SAC: Single-atom catalyst; DACs: diatomic catalysts; WHSV: weight hourly space velocity.

For Pd-Ln/C nanoparticle catalysts, high phenylacetylene conversions were always accompanied by low styrene selectivity, especially at the elevated reaction temperatures, where a large number of styrene would be further hydrogenated to ethylbenzene. Alternatively, in Pd-Ln/C DAC, high styrene selectivity was obtained within a wide temperature range, which might be attributed to the dispersion of Pd active centers. Thus far, there has been consensus that selectivity depends mainly on the adsorption configuration and strength of reactants/intermediates on the catalytic surface, which, in turn, depends on the electronic and geometric configurations of the active sites[55,56]. Nanocatalysts typically exhibit a wide range of size distributions, and nanoparticles can present various facets with diverse atomic structures[57,58]. When concentrating on one nanoparticle, the atom may be located on the edge, terrace, corner sites, or at the interfaces between metal and support, and interact closely with the support[59], and each site experiences specific electronic structures and coordination environments. These multiple active centers would lead to various adsorption modes of the reactants or intermediates, consequently resulting in low catalytic selectivity during catalysis. For SACs or DACs, uniform electronic and geometric structure avoids multiple adsorption modes of reactants/intermediates, thereby improving the selectivity of the target product. A classic example is the adsorption of ethene on Pd(111) surface[55,60], in which ethene is intensely adsorbed as ethylidyne on 3-fold Pd active centers, moderately adsorbed in the di-σ mode onto the bridged Pd active sites, and weakly through π-mode onto the isolated Pd active sites. In our Pd-Ln/C diatomic catalytic system, Pd is the main active site and is dispersed in the form of atoms on the support. After the hydrogenation of phenylacetylene to styrene, styrene is probably adsorbed in a weak π-mode on the isolated Pd, resulting in easy desorption and improved selectivity. Similarly, the $Pd_1$-$Cu_1$/nanodiamond graphene (ND@G) DAC prepared by Huang *et al.* has a 92% ethylene selectivity under complete conversion of

acetylene, which is superior to $Pd_1$/ND@G and $Cu_1$/ND@G SACs[61]. This further supports that the diatomic structures have promising futures in the selective hydrogenation of alkynes.

The presence of small clusters in the DACs may affect the final phenylacetylene hydrogenation reaction performance, but due to the complexity of the catalyst structure, it is difficult to elucidate the specific effect of metals present in different forms in the selective phenylacetylene hydrogenation. It is impossible to establish a reaction system containing pure Pd-Y dual sites to date, we think. Compared with the isolated dual sites, the clusters may bind the styrene more strongly as suggested from the literature[7,8]. This is similar to the adsorption of acetylene on Pt (111) and $Pt_2Sn$ alloy in different intensities[62,63]. For Pt (111), acetylene is adsorbed through strong ethylidyne mode on three-fold Pt sites. For $Pt_2Sn$ alloy, the addition of Sn atoms eliminates all three-fold Pt sites, fragmenting the Pt surface into ensembles of only one or two neighboring Pt atoms. Therefore, acetylene is adsorbed through weak di-σ-mode on the bridged Pt dimers or π-bonded mode on isolated Pt atoms, thus possibly facilitating the desorption of the target product and promoting the selectivity. In our catalytic system, styrene may be adsorbed on clusters through strong ethylidyne mode on three-fold active sites, but adsorbed on dual sites through weak π-bonded mode. Consequently, the existence of the clusters would cause decreasing of styrene selectivity and over-hydrogenation. And 92% styrene selectivity was determined at ~100% conversion under optimized reaction conditions. We believe that the non-uniformed structure is not significant in our system.

To demonstrate that Pd-based rare-earth DACs are more selective for styrene generation than Pd SACs in the hydrogenation of phenylacetylene, we compared the hydrogenation reaction performance of 0.02%Pd/C with that of 0.02%Pd-Ln/C (Ln = Y/Lu). As shown in Figure 3B and C, 0.02%Pd/C SACs achieve complete conversion of phenylacetylene over the reaction temperature range, with a constantly higher conversion of phenylacetylene than the 0.02%Pd-Ln/C (Ln = Y/Lu) DACs. However, the selectivity to styrene decreased from 85% to 64% over the reaction temperature range and was consistently lower than the 0.02%Pd-Ln/C (Ln = Y/Lu) DACs. Moreover, the maximum yield of styrene on 0.02%Pd-Ln/C DACs is higher than that on 0.02%Pd/C SACs [Supplementary Figure 7]. At 393 K, we compared the activity of 0.02%Pd/C SACs and 0.02%Pd-Ln/C (Ln = Y/Lu) DACs [Figure 3D]. The activity of 0.02%Pd-Y/C and 0.02%Pd-Lu/C was 0.03 and 0.07 $mol_{C8H6}/g_{Pd}$/min, respectively, while that of 0.02%Pd/C was 0.87 $mol_{C8H6}/g_{Pd}$/min. The results demonstrated that the activity of 0.02%Pd/C was one order of magnitude higher than that of 0.02%Pd-Ln/C (Ln = Y/Lu), thus leading to excessive hydrogenation of phenylacetylene and reducing styrene selectivity. Meanwhile, we compared the phenylacetylene hydrogenation rate and styrene formation rate of 0.02%Pd-Ln/C DACs and 0.02%Pd/C SACs at similar conversions [Supplementary Figure 8A and B]. The results revealed that styrene selectivity of the 0.02%Pd/C SACs was lower than that of the 0.02%Pd-Ln/C DACs, mainly owing to the hydrogenation rate of phenylacetylene (specific activity) on the 0.02%Pd/C catalyst being greater and resulting in excessive hydrogenation and reduced styrene selectivity. Besides, the results of XANES and EXAFS profiles revealed that rare earth metal Y donated electrons to Pd, making Pd slightly negatively charged. The experiments show that negatively charged Pd can improve the alkene selectivity[64-66]. It appears that the higher electron density of Pd atoms on the catalyst surface would repeal the carbon-carbon double bond of styrene and the π-bonded styrene would desorb facilely[67]. This may be another reason why the styrene selectivity of the 0.02%Pd-Y/C is higher than 0.02%Pd/C.

To further assess the durability of 0.02%Pd-Ln/C (Ln = Y/Lu) in the selective hydrogenation of phenylacetylene, we tested the hydrogenation performance of phenylacetylene at 393 K. As shown in Figure 3E and F, 0.02%Pd-Ln/C (Ln = Y/Lu) showed good durability within 20 h of reaction time on stream (TOS) without any visible decrease in activity and selectivity. Probably, this is mainly due to the presence of rare earth elements and the coordinated foundational groups as described in Scheme 1 within the catalyst,

which enables the catalyst to perform stable catalytic hydrogenation behavior for a long time in the selective hydrogenation of phenylacetylene. Additionally, as displayed in Supplementary Figure 9, 0.02%Pd/C SACs also have long-term catalytic stability, but the selectivity of styrene is obviously lower than that of 0.02%Pd-Ln/C DACs, indicating that the existence of this DAC structure is very important for this selective hydrogenation reaction.

In addition, in order to demonstrate the advantages of Pd-Ln/C DACs in the selective hydrogenation of phenylacetylene, we compared the Pd-Ln/C DACs with Pd-based catalysts in the literature [Supplementary Figure 10]. The Pd-based catalysts reported in the literature with superior activities are all Pd nanoparticle catalysts except $Pd_1$/Ni@G[3]. The literature has shown that in most cases, only the surface atoms of the nanoparticles work as the active components, while the atoms inside the nanoparticles are spectators, leading to great waste in noble metal utilization. The synthesis of highly dispersed precious metals will enhance their atomic efficiency. Reducing the size of metal nanoparticles to single atoms will maximize the availability/utilization of the noble metals and reduce the cost of the catalysts[68,69]. Besides, the modification of Pd with Pb, Se, S and other toxic metals or organic molecules can improve the selectivity of styrene by sacrificing activity, but in the process of hydrogenation, toxic metals or organic molecules will cause catalyst deactivation easily[15,70]. In our Pd-Ln/C diatomic catalytic system, not only is the atomic utilization of metal Pd improved, but the catalyst also maintains good stability during the reaction process.

### Kinetic analysis of phenylacetylene selective hydrogenation

*Dependence of rates on reactant pressures for phenylacetylene hydrogenation*

To investigate the hydrogenation mechanism of phenylacetylene over Pd-Ln/C (Ln = Y/Lu) catalyst, a detailed kinetic analysis was carried out. Prior to that, the internal and external diffusion resistance of the catalyst were excluded by the Koros-Nowak criterion[71] [Supplementary Figure 11A-D].

Table 1 summarizes the reaction order of $C_8H_6$ and $H_2$ over 0.02%Pd-Ln/C (Ln = Y/Lu) and 0.02%Pd/C catalysts. As described in Figure 4A, the hydrogenation rate of $C_8H_6$ increased gradually with the $C_8H_6$ pressure ($[C_8H_6]$, for convenience, the molecule X pressure is expressed as [X]). Specifically, the reaction order of $C_8H_6$ is 0.67 ($r\sim[C_8H_6]^{0.67}$; 0.1-0.8 kPa $C_8H_6$) over 0.02%Pd-Y/C catalyst at 363 K, which is quite similar to the reaction order of $C_8H_6$ at 0.64 ($r\sim[C_8H_6]^{0.64}$; 0.1-0.8 kPa $C_8H_6$) over 0.02%Pd-Lu/C at 363 K. The results suggest that the surface coverages of $C_8H_6$ on 0.02% Pd-Y/C and 0.02% Pd-Lu/C catalysts are quite similar at 363 K. After increasing the reaction temperature, the reaction order of $C_8H_6$ over 0.02%Pd-Y/C and 0.02%Pd-Lu/C catalysts at 373 K is 1.05 ($r\sim[C_8H_6]^{1.05}$; 0.1-0.8 kPa $C_8H_6$) and 0.58 ($r\sim[C_8H_6]^{0.58}$; 0.1-0.8 kPa $C_8H_6$), respectively [Figure 4B]. Compared to 363 K, the surface coverage of $C_8H_6$ is reduced on the 0.02%Pd-Y/C after increasing the temperature to 373 K, while the surface coverage is almost unchanged over 0.02%Pd-Lu/C. As shown in Figure 4A, at 363 K, on the 0.02%Pd-Y/C catalyst, with the increase of $H_2$ pressure, the hydrogenation rate of $C_8H_6$ first slowly grew, and then slightly decreased, in which the reaction order of $H_2$ dropped from 0.55 ($r\sim[H_2]^{0.55}$; 0.5-30 kPa $H_2$) to -0.28 ($r\sim[H_2]^{-0.28}$; 30-50 kPa $H_2$). Clearly, when the partial pressure of $H_2$ is lower than 30 kPa, $C_8H_6$ and $H_2$ are competitively adsorbed on the surface of Pd-Y/C. After raising the partial pressure of $H_2$ to 30 kPa, the negative reaction order of $H_2$ demonstrates that $H_2$ or its derivatives (i.e. $H^*$) would be the dominated surface species over Pd. Similarly, the reaction order of $H_2$ is 0.34 ($r\sim[H_2]^{0.34}$; 0.5-50 kPa $H_2$) over 0.02%Pd-Lu/C catalyst at 363 K. After raising the temperature, the reaction order of $H_2$ varies from 0.49 ($r\sim[H_2]^{0.49}$; 0.5-30 kPa $H_2$) to -0.19 ($r\sim[H_2]^{-0.19}$; 30-50 kPa $H_2$) over 0.02%Pd-Y/C at 373 K [Figure 4B], which reinforces the competitive adsorption between $C_8H_6$ and $H_2$. For 0.02%Pd-Lu/C catalyst, the reaction order of $H_2$ varies from 0.45 ($r\sim[H_2]^{0.45}$; 0.5-30 kPa $H_2$) to -0.21 ($r\sim[H_2]^{-0.21}$; 30-50 kPa $H_2$) at 373 K. Compared with 363 K, the reaction order of $H_2$ on 0.02%Pd-Y/C catalyst did not change significantly with the rise of the reaction temperature, revealing that the coverage of $H_2$ did not change much with temperature. For 0.02%Pd-Lu/C catalyst, the reaction order of $H_2$ becomes more and

**Table 1. Reaction order of phenylacetylene and hydrogen over 0.02%Pd-Ln/C (Ln = Y/Lu) and 0.02%Pd/C catalysts during selective phenylacetylene hydrogenation**

| Catalyst | T/K | $r\text{-}k_{app}[C_8H_6]^x[H_2]^y$ | |
|---|---|---|---|
| | | x | y |
| 0.02%Pd-Y/C | 363 | 0.67 (0.1-0.8 kPa $C_2H_2$) | 0.55 (0.5-30 kPa $H_2$)<br>-0.28 (30-50 kPa $H_2$) |
| | 373 | 1.05 (0.1-0.8 kPa $C_2H_2$) | 0.49 (0.5-30 kPa $H_2$)<br>-0.19 (30-50 kPa $H_2$) |
| 0.02%Pd-Lu/C | 363 | 0.64 (0.1-0.8 kPa $C_2H_2$) | 0.34 (0.5-50 kPa $H_2$) |
| | 373 | 0.58 (0.1-0.8 kPa $C_2H_2$) | 0.45 (0.5-30 kPa $H_2$)<br>-0.21 (30-50 kPa $H_2$) |
| 0.02%Pd/C | 363 | 0.55 (0.1-0.8 kPa $C_8H_6$) | 0.7 (0.5-50 kPa $H_2$) |
| | 373 | 0.49 (0.1-0.8 kPa $C_8H_6$) | 0.68 (0.5-50 kPa $H_2$) |

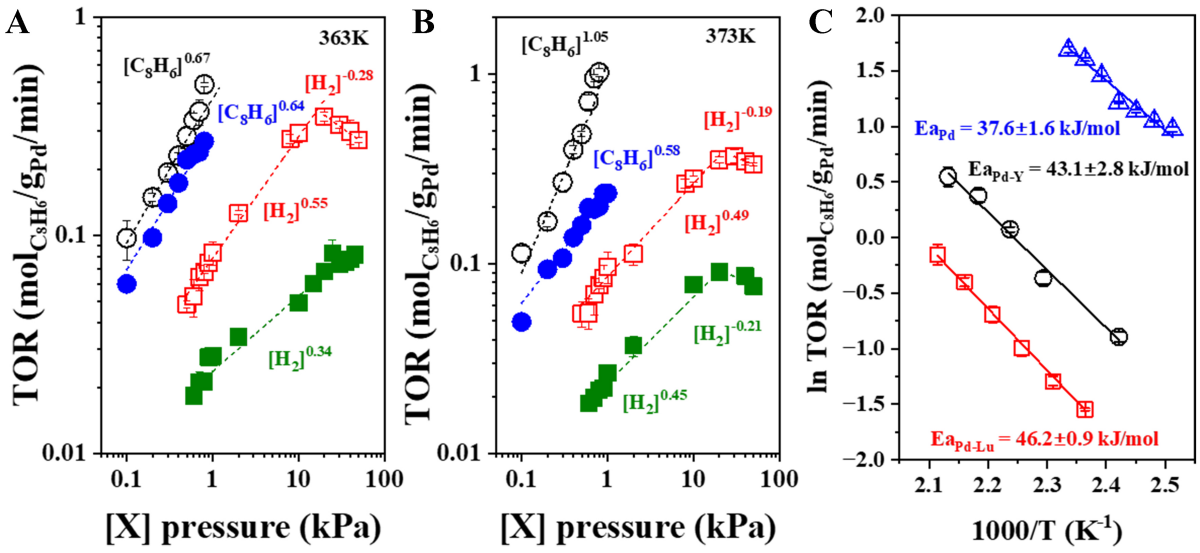


**Figure 4.** Phenylacetylene hydrogenation reaction rates as a function of $H_2$ (red □: 0.02%Pd-Y/C; green ■: 0.02%Pd-Lu/C) (0.5-50 kPa $H_2$, 0.3 kPa $C_8H_6$, 2.784 kPa $C_6H_{12}$, balance with Ar, WHSV = 2,162 $h^{-1}$) and $C_8H_6$ pressures (black ○: 0.02%Pd-Y/C; blue ●: 0.02%Pd-Lu/C) (30 kPa $H_2$, 0.1-0.8 kPa $C_8H_6$, 2.784 kPa $C_6H_{12}$, balance with Ar, WHSV = 2,162 $h^{-1}$) at (A) 363 K and (B) 373 K; (C) Apparent activation energies for phenylacetylene selective hydrogenation over 0.02%Pd-Y/C (black ○), 0.02%Pd-Lu/C (red □) and 0.02%Pd/C (blue △) catalysts. Reaction conditions: 30 kPa $H_2$, 0.3 kPa $C_8H_6$, 2.784 kPa $C_6H_{12}$, balance with Ar, WHSV = 2,162 $h^{-1}$. WHSV: Weight hourly space velocity.

more negative with the rise of temperature, indicating that the coverage of $H_2$ becomes even more dominated at the active Pd site. The similar reaction order of $H_2$ and $C_8H_6$ obtained on 0.02%Pd-Y/C and 0.02%Pd-Lu/C catalysts indicate similar kinetically relevant steps (KRS). Different from 0.02%Pd-Ln/C (Ln = Y/Lu) DACs, independent reaction orders of $H_2$ were observed on 0.02%Pd/C SAC [Supplementary Figure 12], and the reaction orders of $H_2$ on 0.02%Pd/C SAC were 0.7 and 0.68 at 363 and 373 K, respectively, indicating that 0.02%Pd/C SAC and 0.02%Pd-Ln/C (Ln = Y/Lu) DACs may follow separated RDSs. Based on relevant literature reports, the reaction order of $C_8H_6$ is generally between 0 and 1[72-75], which is similar to the reaction order of $C_8H_6$ in our work, demonstrating that the coverage of $C_8H_6$ on the surface of catalyst in the literature and this work is quite similar. While the reaction order of $H_2$ is usually 1 or 1.5[76], which is slightly different from the reaction order of $H_2$ in this work and the detailed correlations between reaction rate and pressures of the reactants might be closely related to the nature of the catalyst and the catalytic reaction conditions applied. Specifically, in this work, the partial pressure of $H_2$ is higher than

that in the literature, which might lead to a higher coverage of $H_2$ in our system.

As displayed in Figure 4C, the apparent activation energies of 0.02%Pd-Y/C and 0.02%Pd-Lu/C DACs were compared, which give 43.1 and 46.2 kJ/mol, respectively. The received rates are in good correlation with the determined apparent reaction barriers, in which the activity of 0.02%Pd-Y/C is similar to that of 0.02%Pd-Lu/C, further demonstrating that these two catalysts probably have the same or similar behavior of hydrogenation. In addition, the activation energies of 0.02%Pd-Ln/C DACs are clearly higher than that of 0.02%Pd/C SAC at ~37.6 kJ/mol, indicating that we are following an activity compromise strategy to fine-tune the selectivity of phenylacetylene hydrogenation that is quite similar to the reported work on acetylene hydrogenation[13,77].

*Mechanism of phenylacetylene selective hydrogenation*

In Combination with the elementary steps of alkyne hydrogenation proposed in the literature[78-80], Podkolzin *et al.* considered the participation of vinylidene and ethylidene species as spectator species when predicting the elementary steps of acetylene hydrogenation on Pt (111) under high coverage of acetylene[78]. Vilé *et al.* and Deng *et al.* did not consider the participation of spectator species when describing the elementary steps of propyne hydrogenation on Ag-based catalysts and acetylene hydrogenation on Ni-based catalysts, respectively[79,80]. In our reaction system, phenylacetylene is at a lower partial pressure (0.3 kPa) than the partial pressure of hydrogen (30 kPa). We believe that the spectator species formed by phenylacetylene might have little effect on the elementary steps of the reaction; at least, they were undetectable. Consequently, the participation of the spectator species is not considered in the elementary steps of phenylacetylene hydrogenation reaction. According to the dissociative (Horiyti-Polanyi)[81] mechanism of phenylacetylene hydrogenation, a series of elementary steps has been proposed and summarized in Scheme 2, where $^*$ represents an unoccupied surface site, $X^*$ denotes the adsorbed species combined with a single Pd active center, and $k_x$ indicates the rate constant of step x. According to the literature, $H_2$ can be adsorbed on Pd single-atom and dissociated into two H atoms in phenylacetylene hydrogenation reaction[3,30]. Besides, it has been proposed that a single metal atom can have multiple active sites. For example, Hoffman *et al.* found that Rh single-atom could adsorb two CO molecules in the study of "CO + NO" reaction on $Rh_1/\gamma$-$Al_2O_3$ catalyst[82]. In addition, Zhang *et al.* studied aldol condensation and esterification on Ti-BEA catalyst, in which single-atom Ti could simultaneously adsorb two acetaldehyde molecules[83] In the 0.02%Pd-Ln/C (Ln = Y/Lu) catalytic system, Pd single-atoms may have different coordination environments (Pd-N, Pd-C, Pd-P, Pd-O, *etc.*). Therefore, Pd single-atoms may have multiple active sites. To simplify the model, we assume that there are more than two (adjacent) active sites on single Pd atoms. In the hydrogenation of phenylacetylene, phenylacetylene molecules are firstly adsorbed on the Pd active centers, and then hydrogen is also adsorbed and dissociated on Pd sites. Dissociated hydrogen atoms will successively combine with adsorbed phenylacetylene molecules to form $C_8H_7^*$ and $C_8H_8^*$ surface species. If the hydrogen barrier of styrene is higher than the desorption barrier of styrene, the styrene produced will desorb and the unoccupied active center will be regenerated. The RDSs of phenylacetylene hydrogenation over 0.02%Pd-Y/C and 0.02%Pd-Lu/C catalysts are discussed as follows:

In Pd-Ln/C DACs, the dissociative chemisorption of $H_2$ occurs predominantly on the Pd sites rather than on the Ln (Ln = Y/Lu) sites or carbon support, and we compared the reaction performance of 0.02%Pd/C, 0.02%Ln/C (Ln = Y/Lu) and carbon support in the selective hydrogenation of phenylacetylene. As shown in Supplementary Figure 13A-D, the conversion of phenylacetylene by 0.02%Ln/C (Ln = Y/Lu) and carbon support was about 2%. The catalytic activity of the 0.02%Ln/C (Ln = Y/Lu) and carbon support was negligible compared with the complete conversion of phenylacetylene by the 0.02%Pd/C catalyst at similar reaction conditions. Meanwhile, it has been shown in the literature that in the selective hydrogenation of

| Step | Reaction | Constant |
|---|---|---|
| 1 | $C_8H_6 + * \rightleftharpoons C_8H_6*$ | $K_1$ |
| 2 | $H_2 + 2* \rightleftharpoons 2H*$ | $K_2$ |
| 3 | $C_8H_6* + H* \rightarrow C_8H_7*+*$ | $k_3$ |
| 4 | $C_8H_7* + H* \rightleftharpoons C_8H_8*+*$ | $K_4$ |
| 5 | $C_8H_8* \rightleftharpoons C_8H_8+*$ | $K_5$ |

**Scheme 2.** The elementary steps of the dissociative (Horiuti-Polanyi) mechanism.

alkyne over a second metal alloyed/modified Pd SAC, the mainly active site of catalyst is the single-atom Pd[11,67]. Thus, the hydrogenation reaction of phenylacetylene was assumed to mainly occur on the Pd singe-atom active site. Assuming the adsorption of reactants and the desorption of products in the reaction step are quasi-equilibrated (QE), and "$C_8H_6^*$ + $H^*$" is kinetically relevant, the active species can be represented as below:

$$[L_{Pd}] = [*] + [H*] + [C_8H_6*] + [C_8H_7*] + [C_8H_8*] \tag{5}$$

And the hydrogenation rate of $C_8H_6$ will be expressed as:

$$\frac{r}{[L_{Pd}]} = \frac{k_3[C_8H_6*][H*]}{[L_{Pd}]^2} \tag{6}$$

Considering the QE hypothesis of $C_8H_6$ adsorption, $H_2$ dissociation, $C_8H_8$ desorption and equilibrium of surface active centers:

$$[H*] = \sqrt{K_2}[H_2]^{\frac{1}{2}}[*] \tag{7}$$

$$[C_8H_6*] = K_1[C_8H_6][*] \tag{8}$$

$$[C_8H_7*] = \frac{[C_8H_8]}{K_4K_5\sqrt{K_2}[H_2]^{\frac{1}{2}}}[*] \tag{9}$$

$$[C_8H_8*] = \frac{[C_8H_8][*]}{K_5} \tag{10}$$

Supplementary Note 1 gives a complete deduction of the rate expression, and Equation (6) can be expressed as:

$$\frac{r}{[L_{Pd}]} = \frac{k_3K_1\sqrt{K_2}[H_2]^{\frac{1}{2}}[C_8H_6]}{\left(1 + \sqrt{K_2}[H_2]^{\frac{1}{2}} + K_1[C_8H_6] + \frac{[C_8H_8]}{K_4K_5\sqrt{K_2}[H_2]^{\frac{1}{2}}} + \frac{[C_8H_8]}{K_5}\right)^2} \tag{11}$$

Where the molecular term represents a series of steps to form the product, and the denominator represents the balance of active sites on the surface occupied by the reactants and their derivatives, as well as some

unoccupied active sites. When [$C_8H_6$] is low, the amount of vacancy sites ("*", most likely to be occupied by $H_2$ and $C_8H_6$) may be larger than the quantity of adsorbed $C_8H_6$-derived species, and Equation (10) predicates that the $C_8H_8$ turnover rate is first-order dependent on $C_8H_6$ pressure. When [$C_8H_6$] is higher, the $C_8H_6$-derived species will turn into the most abundant reaction intermediates (MARIs), and Equation (10) suggests that the rate is negligible or negatively first-order dependent with respect to [$C_8H_6$]. Similarly, after hypothesizing various species as MASIs, the rate expression would be simplified to half-order or negative half-order in $H_2$, which is consistent with the observed pressure dependence very well. Therefore, the "$C_8H_6^*$ + $H^*$" (step 3) may be the RDS of 0.02%Pd-Y/C and 0.02%Pd-Lu/C DACs. In addition, we have also studied the RDS of phenylacetylene hydrogenation reaction on 0.02%Pd/C SAC (Supplementary Note 2 for details). The results show that the RDS of 0.02%Pd/C is probably "$C_8H_7^*$ + $H^*$", which is in good agreement with our previous research that the RDS of acetylene hydrogenation reaction on Pd-based catalyst varies with the catalytic activity[84].

According to the literature, modification of the core metal with a second metal atom can change the coordination environment and electronic structure of the latter[85-89]. For example, in the selective hydrogenation of acetylene on $Pd_1$-$Cu_1$/ND@G DACs[61], compared to $Pd_1$/ND@G and $Cu_1$/ND@G SACs, $Pd_1$-$Cu_1$/ND@G DACs exhibit a geometry advantage in simultaneously adsorbing acetylene and hydrogen, thereby transforming the competitive adsorption of reactants into relatively non-competitive adsorption. In addition, the electronic structure of $Pd_1$-$Cu_1$ atomic pairs facilitates the adsorption of reactants, altering the reaction pathway and providing a lower barrier from acetylene to ethylene. Similarly, in bimetallic site mesoporous silica (MS) stabilized Pd-Ru@ZIF-8 catalyst for selective hydrogenation of phenylacetylene[38], Pd atoms facilitate the formation of styrene, while Ru atoms facilitate the desorption of styrene. The synergistic effect of Pd and Ru atoms promotes the activation of phenylacetylene, with better catalytic performance than MS Pd@ZIF-8 and MS Ru@ZIF-8 catalysts. Combing literature reports and experimental results, in our Pd-based rare-earth DAC system, the Pd atom probably contributes to the activation of phenylacetylene, while the rare-earth element Ln (Y/Lu) helps stabilize this isolated structure and possibly facilitate the desorption of styrene since the desorption of styrene were determined to be facile over highly dispersed structures[38,61], thus avoiding further hydrogenation of styrene. The electronic modification of the Ln elements against isolated Pd is quite complex and would be further explained in our future work.

To confirm that the dissociation of $H_2$ elementary step is not the RDS for 0.02%Pd-Y/C and 0.02%Pd-Lu/C catalysts, we tentatively assumed that dissociation of $H_2$ is the RDS, and detailed kinetic derivation was included in Supplementary Note 1. Probably, the dissociation of $H_2$ is facile and will not be the RDS in our reaction system. And it is reported that hydrogen is prone to dissociation on metal Pd[81], and in the kinetic model, it is recognized that the dissociation of hydrogen is not the RDS[90].

To verify the reaction model proposed, the experimental rates were systematically correlated to the predicated ones over 0.02%Pd-Y/C and 0.02%Pd-Lu/C catalysts following parity plot fittings, and the corresponding kinetic constants were obtained at the same time. The parity plots over 0.02%Pd-Y/C and 0.02%Pd-Lu/C catalysts are shown in Supplementary Figure 14. For both catalysts, the experimental and predicated rates are well distributed on a straight line with a slope of 1 and an intercept of 0, indicating that the dissociation mechanism of phenylacetylene on Pd-based rare earth DACs is reasonable. The rate constants ($k_3$) and equilibrium constants ($K_1$, $K_2$) acquired by regression are shown in Table 2. The equilibrium constants of 0.02%Pd-Y/C and 0.02%Pd-Lu/C catalysts acquired by parity fitting are very close, demonstrating that the transition state energy barriers for the adsorption of reactants and hydrogenation of reaction intermediates on the two catalysts are quite similar. Besides, these regressed kinetic constants acquired by parity fitting can be used to estimate the coverages of different species, where at different

**Table 2. The equilibrium constants and rate constants of $C_8H_6$ hydrogenation over 0.02%Pd-Y/C and 0.02%Pd-Lu/C catalysts at 363-373 K determined by parity fittings**

| Sample | T/K | Equilibrium and rate constants | | |
|---|---|---|---|---|
| | | $k_3/s^{-1}$ | $K_1/kPa^{-1}$ | $K_2/kPa^{-1}$ |
| 0.02%Pd-Y/C | 363 | 4.99 | 1.31 | 0.02 |
| | 373 | 6.61 | 1.12 | 0.01 |
| 0.02%Pd-Lu/C | 363 | 0.67 | 3.68 | 0.03 |
| | 373 | 1.25 | 1.50 | 0.02 |

reaction temperatures, the regressed equilibrium constant $K_1$ of phenylacetylene adsorption acquired is always more significant than the $K_2$ of hydrogen. For example, for 0.02%Pd-Y/C catalyst, the $K_1$ values at 363 and 373 K are 1.31 and 1.12, respectively, which are obviously larger than the $K_2$ values at 363 and 373 K (respectively at 0.02 and 0.01), the results suggest that $C_8H_6^*$ is probably the MARIs of this reaction during catalysis, which is in good consistency with our hypothesis according to the kinetic evaluations.

### Thermodynamic discussion

Kinetic analysis suggested that for the 0.02%Pd-Ln/C (Ln = Y/Lu) DAC with high styrene selectivity, "$C_8H_6^*$ + $H^*$" elementary step is probably the RDS of this reaction. In addition, when the partial pressure of $H_2$ is below 30 kPa, $C_8H_6$ and $H_2$ compete for the active sites from the surface of the catalyst, and when the partial pressure of $H_2$ is above 30 kPa, $H_2$ is the main adsorbed species. At the same time, the results of parity fitting between the experimental rates and the predicated ones also verified the correctness of our catalytic model. Moreover, researchers can also estimate the thermodynamic parameters in the catalytic process through parity fitting. For example, in the selective hydrogenation of acetylene previously studied in our group[84], the thermodynamic parameters were determined by parity fitting and some isothermal adsorption experiments. Therefore, we would like to understand the phenylacetylene semi-hydrogenation in a similar way, which would undoubtedly provide additional information on the basis of DFT calculations.

As the 0.02%Pd-Y/C and 0.02%Pd-Lu/C catalysts have similar activation energies and probably the same RDS, we chose the 0.02%Pd-Y/C catalyst as an example to determine the relevant energy of every reactive intermediate before and after $C_8H_6$ hydrogenation in the transition state to reflect the change in specific energy along $C_8H_6$ hydrogenation. Combining our own kinetic analysis with the theoretical calculation[91], the entire hydrogenation procedure over 0.02%Pd-Y/C sample was described following the transition state theory (TST) [Figure 5]. Supplementary Table 5 lists the energy parameters acquired through parity fitting and $H_2$ isothermal adsorption. The detailed derivation results can be found in the Supplementary Note 3. First of all, we set the activation enthalpy of gaseous $C_8H_6$ at 0.3 kPa and $H_2$ at 30 kPa as 0 kJ/mol. As expected, phenylacetylene hydrogenation is an exothermic reaction. According to the parity fitting and isothermal $H_2$ adsorption experiments [Supplementary Figure 15A and B], the adsorption heats of $C_8H_6$ and $H_2$ on 0.02%Pd-Y/C catalysts are respectively at 45.6 and 17.2 kJ/mol. These adsorption heats are quite similar to that reported in the literature[92]. For instance, Cheng *et al.* studied the hydrogenation of benzaldehyde on Pd/C catalyst, and the $H_2$ adsorption heat measured by $H_2$ isothermal adsorption experiment was about 14 kJ/mol[92]. In addition, Li *et al.* calculated the adsorption heat of $C_8H_6$ on different Pd-based catalysts by DFT calculations and suggested that the value should be within the range of 27.6-81.1 kJ/mol[38], which matches the value we determined quite well. For the transition state potential of $C_8H_6$ hydrogenation, it appears that the potential of $C_8H_6$ hydrogenation is essentially increasing gradually, even though the whole transition state energy barriers cannot be determined. The apparent activation energy of the 0.02%Pd-Y/C DAC determined experimentally is lower than the intrinsic transition state energy barrier for phenylacetylene hydrogenation determined in Figure 5. According to the literature, the apparent

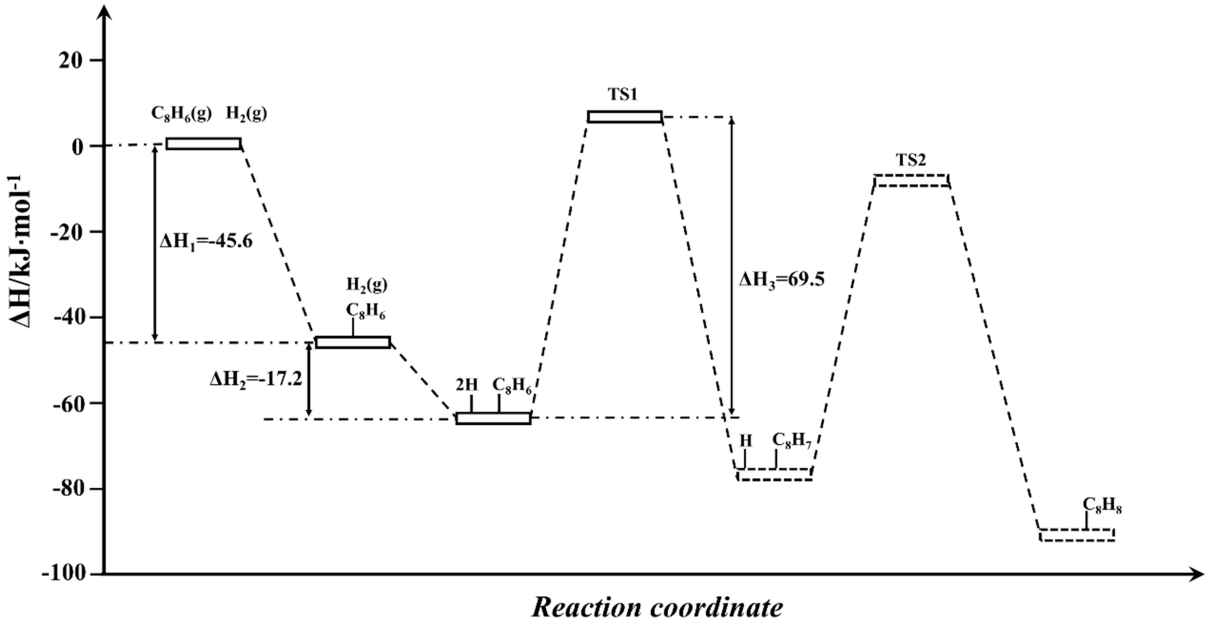


**Figure 5.** Simplified energy diagram for hydrogenation of phenylacetylene over 0.02%Pd-Y/C catalyst. The solid rectangle represents the real results measured based on the kinetic and thermodynamic parameters, and the dotted rectangle represents the assumed values.

activation energy of phenylacetylene hydrogenation on Pd-based catalysts ranges from 30 to 70 kJ/mol [Supplementary Table 6]. The apparent activation energy of the catalyst acquired in the experiment conforms to the range of activation energies reported[3,93,94]. In the relevant theoretical calculation results, the intrinsic transition state energy barrier of phenylacetylene hydrogenation is usually greater than 100 kJ/mol, which is much higher than the apparent activation energy of the catalyst measured experimentally. Generally, the theoretical calculation focuses on the energy difference between the ground state and the transition state[38,91,95], which is in good agreement with the values determined in this work. In addition, the activation enthalpy of the intermediates in phenylacetylene hydrogenation displays a downward tendency, which could cause the intrinsic energy barrier of phenylacetylene hydrogenation to be greater than the determined apparent energy barrier. Through the measured parameters of kinetic and thermodynamic, the TST explains the whole process of phenylacetylene hydrogenation reaction well.

## CONCLUSION

In brief, we developed Pd-based rare earth DACs (0.02%Pd-Ln/C, Ln = Y/Lu) for the selective hydrogenation of phenylacetylene in this work. The XANES and EXAFS characterizations showed that the rare earth metal Y donates some electrons to the adjacent isolated Pd, making Pd slightly negatively charged and promoting the styrene selectivity. Through the synergistic effect between diatomic Pd and Ln (Ln = Y/Lu), 92% styrene selectivity was obtained upon complete conversion of phenylacetylene. Meanwhile, the 0.02%Pd-Ln/C (Ln = Y/Lu) DACs can maintain the stability and durability for up to 20 h at 393 K. Kinetic analysis and apparent activation energy assessment suggest that the 0.02%Pd-Y/C and 0.02%Pd-Lu/C DACs probably follow the same reaction path and had the same RDS, that is, "$C_8H_6^*$ + $H^*$". Besides, $C_8H_6^*$ and $H^*$ were the primary adsorbed species on 0.02%Pd-Ln/C (Ln = Y/Lu). The parameters of kinetic and thermodynamic were acquired by parity fitting and isothermal $H_2$ adsorption experiment, the energy relationship along the hydrogenation elementary steps of phenylacetylene was quantitatively described, and the entire hydrogenation process of the phenylacetylene hydrogenation was interpreted by the TST well. The overall reaction performance of selective hydrogenation of phenylacetylene to styrene was selectively improved by the diatomic structure of Pd-Ln.

## DECLARATIONS

### Acknowledgments

Special thanks to Guo JQ from the research group for assisting in the characterization testing of dual-atomic catalysts during the article revision stage.

### Authors' contributions

Conceptualization, investigation, methodology, data curation, formal analysis, writing - original draft: Che L, Zhong Z

Conceptualization, funding acquisition, resources, supervision, project administration, writing - review and editing: Zhang H, Cui P, Du Y

### Availability of data and materials

Experimental details on synthesis, characterization, and catalysis are available in the Supplementary Materials.

### Financial support and sponsorship

We gratefully acknowledge the support from the National Science Fund for Distinguished Young Scholars (22425503), the National Natural Science Foundation of China (22371131, 22172078), the 111 Project (B18030) from China, the Outstanding Youth Project of Tianjin Natural Science Foundation (20JCJQJC00130), the Key Laboratory of Rare Earths, Chinese Academy of Sciences, and the Haihe Laboratory of Sustainable Chemical Transformations for financial support.

### Conflicts of interest

All authors declared that there are no conflicts of interest.

### Ethical approval and consent to participate

Not applicable.

### Consent for publication

Not applicable.



## REFERENCES

1. Crespo-Quesada M, Cárdenas-Lizana F, Dessimoz A, Kiwi-Minsker L. Modern trends in catalyst and process design for alkyne hydrogenations. *ACS Catal* 2012;2:1773-86. DOI
2. Tang J, Liu P, Liu X, et al. In situ encapsulation of Pt nanoparticles within pure silica TON zeolites for space-confined selective hydrogenation. *ACS Appl Mater Interfaces* 2020;12:11522-32. DOI PubMed
3. Zhao L, Qin X, Zhang X, et al. A magnetically separable Pd single-atom catalyst for efficient selective hydrogenation of phenylacetylene. *Adv Mater* 2022;34:e2110455. DOI PubMed
4. Deng D, Yang Y, Gong Y, Li Y, Xu X, Wang Y. Palladium nanoparticles supported on mpg-$C_3N_4$ as active catalyst for semihydrogenation of phenylacetylene under mild conditions. *Green Chem* 2013;15:2525. DOI
5. Shao L, Huang X, Teschner D, Zhang W. Gold supported on graphene oxide: an active and selective catalyst for phenylacetylene hydrogenations at low temperatures. *ACS Catal* 2014;4:2369-73. DOI
6. Liu Y, Guo W, Li X, Jiang P, Zhang N, Liang M. Copper single-atom-covered Pt nanoparticles for selective hydrogenation of phenylacetylene. *ACS Appl Nano Mater* 2021;4:5292-300. DOI
7. Liu K, Qin R, Zheng N. Insights into the interfacial effects in heterogeneous metal nanocatalysts toward selective hydrogenation. *J Am Chem Soc* 2021;143:4483-99. DOI PubMed

8. Zhang L, Zhou M, Wang A, Zhang T. Selective hydrogenation over supported metal catalysts: from nanoparticles to single atoms. *Chem Rev* 2020;120:683-733. DOI PubMed
9. Teschner D, Borsodi J, Wootsch A, et al. The roles of subsurface carbon and hydrogen in palladium-catalyzed alkyne hydrogenation. *Science* 2008;320:86-9. DOI PubMed
10. Choe K, Zheng F, Wang H, et al. Fast and selective semihydrogenation of alkynes by palladium nanoparticles sandwiched in metal-organic frameworks. *Angew Chem Int Ed Engl* 2020;59:3650-7. DOI PubMed
11. Pei GX, Liu XY, Wang A, et al. Ag alloyed Pd single-atom catalysts for efficient selective hydrogenation of acetylene to ethylene in excess ethylene. *ACS Catal* 2015;5:3717-25. DOI
12. Osswald J, Giedigkeit R, Jentoft R, et al. Palladium–gallium intermetallic compounds for the selective hydrogenation of acetylene: Part I: preparation and structural investigation under reaction conditions. *J Catal* 2008;258:210-8. DOI
13. Luo Y, Alarcón Villaseca S, Friedrich M, Teschner D, Knop-Gericke A, Armbrüster M. Addressing electronic effects in the semi-hydrogenation of ethyne by $InPd_2$ and intermetallic Ga–Pd compounds. *J Catal* 2016;338:265-72. DOI
14. Chen X, Peng M, Cai X, et al. Regulating coordination number in atomically dispersed Pt species on defect-rich graphene for n-butane dehydrogenation reaction. *Nat Commun* 2021;12:2664. DOI PubMed PMC
15. Schoenbaum CA, Schwartz DK, Medlin JW. ChemInform abstract: controlling the surface environment of heterogeneous catalysts using self-assembled monolayers. *ChemInform* 2014;45:chin.201425241. DOI
16. Shen C, Ji Y, Wang P, et al. Interface confinement in metal nanosheet for high-efficiency semi-hydrogenation of alkynes. *ACS Catal* 2021;11:5231-9. DOI
17. Miyazaki M, Furukawa S, Takayama T, Yamazoe S, Komatsu T. Surface modification of PdZn nanoparticles via galvanic replacement for the selective hydrogenation of terminal alkynes. *ACS Appl Nano Mater* 2019;2:3307-14. DOI
18. Kaiser SK, Chen Z, Faust Akl D, Mitchell S, Pérez-Ramírez J. Single-atom catalysts across the periodic table. *Chem Rev* 2020;120:11703-809. DOI PubMed
19. Gan T, Wang D. Atomically dispersed materials: ideal catalysts in atomic era. *Nano Res* 2024;17:18-38. DOI
20. Zhu P, Feng W, Zhao D, et al. p-Block bismuth nanoclusters sites activated by atomically dispersed bismuth for tandem boosting electrocatalytic hydrogen peroxide production. *Angew Chem Int Ed Engl* 2023;62:e202304488. DOI PubMed
21. Zhao D, Chen Z, Yang W, et al. MXene ($Ti_3C_2$) vacancy-confined single-atom catalyst for efficient functionalization of $CO_2$. *J Am Chem Soc* 2019;141:4086-93. DOI PubMed
22. Wang A, Li J, Zhang T. Heterogeneous single-atom catalysis. *Nat Rev Chem* 2018;2:65-81. DOI
23. Deng D, Chen X, Yu L, et al. A single iron site confined in a graphene matrix for the catalytic oxidation of benzene at room temperature. *Sci Adv* 2015;1:e1500462. DOI PubMed PMC
24. Huang F, Deng Y, Chen Y, et al. Atomically dispersed Pd on nanodiamond/graphene hybrid for selective hydrogenation of acetylene. *J Am Chem Soc* 2018;140:13142-6. DOI PubMed
25. Hannagan RT, Giannakakis G, Flytzani-Stephanopoulos M, Sykes ECH. Single-atom alloy catalysis. *Chem Rev* 2020;120:12044-88. DOI PubMed
26. Huang F, Deng Y, Chen Y, et al. Anchoring $Cu_1$ species over nanodiamond-graphene for semi-hydrogenation of acetylene. *Nat Commun* 2019;10:4431. DOI PubMed PMC
27. Liu Y, Wang B, Fu Q, et al. Polyoxometalate-based metal-organic framework as molecular sieve for highly selective semi-hydrogenation of acetylene on isolated single Pd atom sites. *Angew Chem Int Ed Engl* 2021;60:22522-8. DOI PubMed
28. Guo Y, Huang Y, Zeng B, et al. Photo-thermo semi-hydrogenation of acetylene on $Pd_1/TiO_2$ single-atom catalyst. *Nat Commun* 2022;13:2648. DOI PubMed PMC
29. Fu B, Mccue AJ, Liu Y, et al. Highly selective and stable isolated non-noble metal atom catalysts for selective hydrogenation of acetylene. *ACS Catal* 2022;12:607-15. DOI
30. Yang F, Ding S, Song H, Yan N. Single-atom Pd dispersed on nanoscale anatase $TiO_2$ for the selective hydrogenation of phenylacetylene. *Sci China Mater* 2020;63:982-92. DOI
31. Zhang W, Chao Y, Zhang W, et al. Emerging dual-atomic-site catalysts for efficient energy catalysis. *Adv Mater* 2021;33:e2102576. DOI PubMed
32. Wang D, Li Y. Bimetallic nanocrystals: liquid-phase synthesis and catalytic applications. *Adv Mater* 2011;23:1044-60. DOI PubMed
33. Sankar M, Dimitratos N, Miedziak PJ, Wells PP, Kiely CJ, Hutchings GJ. Designing bimetallic catalysts for a green and sustainable future. *Chem Soc Rev* 2012;41:8099-139. DOI PubMed
34. Zhang L, Xie Z, Gong J. Shape-controlled synthesis of Au-Pd bimetallic nanocrystals for catalytic applications. *Chem Soc Rev* 2016;45:3916-34. DOI PubMed
35. Zhu X, Guo Q, Sun Y, et al. Optimising surface d charge of AuPd nanoalloy catalysts for enhanced catalytic activity. *Nat Commun* 2019;10:1428. DOI PubMed PMC
36. Li H, Shin K, Henkelman G. Effects of ensembles, ligand, and strain on adsorbate binding to alloy surfaces. *J Chem Phys* 2018;149:174705. DOI PubMed
37. Yang X, Tat T, Libanori A, et al. Single-atom catalysts with bimetallic centers for high-performance electrochemical $CO_2$ reduction. *Mater Today* 2021;45:54-61. DOI
38. Li Z, Hu M, Liu J, et al. Mesoporous silica stabilized MOF nanoreactor for highly selective semi-hydrogenation of phenylacetylene via synergistic effect of Pd and Ru single site. *Nano Res* 2022;15:1983-92. DOI

39. Zeng Z, Xu Y, Zhang Z, et al. Rare-earth-containing perovskite nanomaterials: design, synthesis, properties and applications. *Chem Soc Rev* 2020;49:1109-43. DOI PubMed
40. Xu J, Chen X, Xu Y, Du Y, Yan C. Ultrathin 2D rare-earth nanomaterials: compositions, syntheses, and applications. *Adv Mater* 2020;32:e1806461. DOI PubMed
41. Kim C, Dionigi F, Beermann V, Wang X, Möller T, Strasser P. Alloy nanocatalysts for the electrochemical oxygen reduction (ORR) and the direct electrochemical carbon dioxide reduction reaction ($CO_2$ RR). *Adv Mater* 2019;31:e1805617. DOI PubMed
42. Jong Yoo S, Kim SK, Jeon TY, et al. Enhanced stability and activity of Pt-Y alloy catalysts for electrocatalytic oxygen reduction. *Chem Commun* 2011;47:11414-6. DOI PubMed
43. Yoo SJ, Hwang SJ, Lee J, et al. Promoting effects of La for improved oxygen reduction activity and high stability of Pt on Pt–La alloy electrodes. *Energy Environ Sci* 2012;5:7521. DOI
44. Escudero-Escribano M, Verdaguer-Casadevall A, Malacrida P, et al. $Pt_5Gd$ as a highly active and stable catalyst for oxygen electroreduction. *J Am Chem Soc* 2012;134:16476-9. DOI PubMed
45. Kanady JS, Leidinger P, Haas A, et al. Synthesis of $Pt_3Y$ and other early-late intermetallic nanoparticles by way of a molten reducing agent. *J Am Chem Soc* 2017;139:5672-5. DOI PubMed
46. Velázquez-Palenzuela A, Masini F, Pedersen AF, et al. The enhanced activity of mass-selected Pt Gd nanoparticles for oxygen electroreduction. *J Cataly* 2015;328:297-307. DOI
47. Brandiele R, Durante C, Grądzka E, et al. One step forward to a scalable synthesis of platinum–yttrium alloy nanoparticles on mesoporous carbon for the oxygen reduction reaction. *J Mater Chem A* 2016;4:12232-40. DOI
48. Cui P, Wu C, Du J, Luo G, Huang Z, Zhou S. Three-coordinate Pd(0) with rare-earth metalloligands: synergetic CO activation and double P-C bond cleavage-formation reactions. *Inorg Chem* 2021;60:9688-99. DOI PubMed
49. Lee HG, Milner PJ, Buchwald SL. An improved catalyst system for the Pd-catalyzed fluorination of (hetero)aryl triflates. *Org Lett* 2013;15:5602-5. DOI PubMed PMC
50. Liu J, Kong X, Zheng L, Guo X, Liu X, Shui J. Rare earth single-atom catalysts for nitrogen and carbon dioxide reduction. *ACS Nano* 2020;14:1093-101. DOI PubMed
51. Zhang E, Hu X, Meng L, et al. Single-atom yttrium engineering janus electrode for rechargeable Na-S batteries. *J Am Chem Soc* 2022;144:18995-9007. DOI PubMed
52. Tan W, Xie S, Le D, et al. Fine-tuned local coordination environment of Pt single atoms on ceria controls catalytic reactivity. *Nat Commun* 2022;13:7070. DOI PubMed PMC
53. Muravev V, Spezzati G, Su Y, et al. Interface dynamics of Pd–$CeO_2$ single-atom catalysts during CO oxidation. *Nat Catal* 2021;4:469-78. DOI
54. Ye TN, Lu Y, Xiao Z, et al. Palladium-bearing intermetallic electride as an efficient and stable catalyst for Suzuki cross-coupling reactions. *Nat Commun* 2019;10:5653. DOI PubMed PMC
55. Hamm G, Schmidt T, Breitbach J, Franke D, Becker C, Wandelt K. The adsorption of ethene on Pd(111) and ordered Sn/Pd(111) surface alloys. *Zeitschrift für Physikalische Chemie* 2009;223:209-32. DOI
56. Lear T, Marshall R, Lopez-Sanchez JA, et al. The application of infrared spectroscopy to probe the surface morphology of alumina-supported palladium catalysts. *J Chem Phys* 2005;123:174706. DOI PubMed
57. Zhou K, Li Y. Catalysis based on nanocrystals with well-defined facets. *Angew Chem Int Ed Engl* 2012;51:602-13. DOI PubMed
58. Hori Y, Takahashi I, Koga O, Hoshi N. Selective formation of C2 compounds from electrochemical reduction of $CO_2$ at a series of copper single crystal electrodes. *J Phys Chem B* 2002;106:15-7. DOI
59. Brodersen SH, Grønbjerg U, Hvolbæk B, Schiøtz J. Understanding the catalytic activity of gold nanoparticles through multi-scale simulations. *J Catal* 2011;284:34-41. DOI
60. Li M, Shen J. Microcalorimetric studies of $O_2$ and $C_2H_4$ adsorption on Pd/$SiO_2$ catalysts modified by Cu and Ag. *Thermochim Acta* 2001;379:45-50. DOI
61. Huang F, Peng M, Chen Y, et al. Low-temperature acetylene semi-hydrogenation over the $Pd_1$-$Cu_1$ dual-atom catalyst. *J Am Chem Soc* 2022;144:18485-93. DOI PubMed
62. Gao J, Zhao H, Yang X, Koel BE, Podkolzin SG. Controlling acetylene adsorption and reactions on Pt–Sn catalytic surfaces. *ACS Catal* 2013;3:1149-53. DOI
63. Gao J, Zhao H, Yang X, Koel BE, Podkolzin SG. Geometric requirements for hydrocarbon catalytic sites on platinum surfaces. *Angew Chem Int Ed Engl* 2014;53:3641-4. DOI PubMed
64. Sanville E, Kenny SD, Smith R, Henkelman G. Improved grid-based algorithm for Bader charge allocation. *J Comput Chem* 2007;28:899-908. DOI PubMed
65. Huang DC, Chang KH, Pong WF, Tseng PK, Hung KJ, Huang WF. Effect of Ag-promotion on Pd catalysts by XANES. *Catal Lett* 1998;53:155-9. DOI
66. Lamb RN, Ngamsom B, Trimm DL, Gong B, Silevston PL, Praserthdam P. Surface characterisation of Pd-Ag/$Al_2O_3$ catalysts for acetylene hydrogenation using an improved XPS procedure. *Appl Catal A Gen* 2004;268:43-50. DOI
67. Pei GX, Liu XY, Yang X, et al. Performance of Cu-alloyed Pd single-atom catalyst for semihydrogenation of acetylene under simulated front-end conditions. *ACS Catal* 2017;7:1491-500. DOI
68. Qiao B, Wang A, Yang X, et al. Single-atom catalysis of CO oxidation using Pt1/FeOx. *Nat Chem* 2011;3:634-41. DOI PubMed
69. Yang XF, Wang A, Qiao B, Li J, Liu J, Zhang T. Single-atom catalysts: a new frontier in heterogeneous catalysis. *Acc Chem Res*

2013;46:1740-8. DOI PubMed

70. Vilé G, Almora-Barrios N, Mitchell S, López N, Pérez-Ramírez J. From the Lindlar catalyst to supported ligand-modified palladium nanoparticles: selectivity patterns and accessibility constraints in the continuous-flow three-phase hydrogenation of acetylenic compounds. *Chemistry* 2014;20:5926-37. DOI PubMed
71. Madon RJ, Boudart M. Experimental criterion for the absence of artifacts in the measurement of rates of heterogeneous catalytic reactions. *Ind Eng Chem Fund* 1982;21:438-47. DOI
72. Jackson S, Shaw LA. The liquid-phase hydrogenation of phenyl acetylene and styrene on a palladium/carbon catalyst. *Appl Catal A Gen* 1996;134:91-9. DOI
73. Cabello J, Campelo J, Garcia A, Luna D, Marinas J. $AlPO_4$-supported rhodium catalysts. *J Catal* 1985;94:1-9. DOI
74. Campelo JM, Garcia A, Luna D, Marinas JM. Liquid-phase hydrogenation on new $AlPO_4$−$SiO_2$ supported rhodium catalysts. *React Kinet Catal Lett* 1982;21:209-12. DOI
75. Madon RJ, O'Connell JP, Boudart M. Catalytic hydrogenation of cyclohexene: Part II. Liquid phase reaction on supported platinum in a gradientless slurry reactor. *AIChE J* 1978;24:904-11. DOI
76. Wilhite BA, Mccready MJ, Varma A. Kinetics of phenylacetylene hydrogenation over Pt/γ-$Al_2O_3$ catalyst. *Ind Eng Chem Res* 2002;41:3345-50. DOI
77. Sachtler WMH. Chemisorption complexes on alloy surfaces. *Catal Rev* 1976;14:193-210. DOI
78. Podkolzin SG, Alcalá R, Dumesic JA. Density functional theory studies of acetylene hydrogenation on clean, vinylidene- and ethylidyne-covered Pt(111) surfaces. *J Mol Catal A Chem* 2004;218:217-27. DOI
79. Vilé G, Baudouin D, Remediakis IN, Copéret C, López N, Pérez-Ramírez J. Silver nanoparticles for olefin production: new insights into the mechanistic description of propyne hydrogenation. *ChemCatChem* 2013;5:3750-9. DOI
80. Deng X, Bai R, Chai Y, Hu Z, Guan N, Li L. Homogeneous-like alkyne selective hydrogenation catalyzed by cationic nickel confined in zeolite. *CCS Chem* 2022;4:949-62. DOI
81. Horiuti I, Polanyi M. Exchange reactions of hydrogen on metallic catalysts. *Trans Faraday Soc* 1934;30:1164-72. DOI
82. Hoffman AJ, Asokan C, Gadinas N, et al. Experimental and theoretical characterization of Rh single atoms supported on γ-$Al_2O_3$ with varying hydroxyl contents during NO reduction by CO. *ACS Catal* 2022;12:11697-715. DOI
83. Zhang Z, Berdugo-Díaz CE, Bregante DT, Zhang H, Flaherty DW. Aldol condensation and esterification over Ti-substituted *BEA zeolite: mechanisms and effects of pore hydrophobicity. *ACS Catal* 2022;12:1481-96. DOI
84. Che L, Guo J, He Z, Zhang H. Evidence of rate-determining step variation along reactivity in acetylene hydrogenation: a systematic kinetic study on elementary steps, kinetically relevant(s) and active species. *J Catal* 2022;414:336-48. DOI
85. He Z, He K, Robertson AW, et al. Atomic structure and dynamics of metal dopant pairs in graphene. *Nano Lett* 2014;14:3766-72. DOI PubMed
86. Liu C, Li T, Dai X, et al. Catalytic activity enhancement on alcohol dehydrogenation via directing reaction pathways from single- to double-atom catalysis. *J Am Chem Soc* 2022;144:4913-24. DOI PubMed
87. Zhao X, Wang F, Kong XP, Fang R, Li Y. Dual-metal hetero-single-atoms with different coordination for efficient synergistic catalysis. *J Am Chem Soc* 2021;143:16068-77. DOI PubMed
88. Zhang X, Zhang M, Deng Y, et al. A stable low-temperature $H_2$-production catalyst by crowding Pt on α-MoC. *Nature* 2021;589:396-401. DOI PubMed
89. Li S, Cao R, Xu M, et al. Atomically dispersed Ir/α-MoC catalyst with high metal loading and thermal stability for water-promoted hydrogenation reaction. *Natl Sci Rev* 2022;9:nwab026. DOI PubMed PMC
90. Borodziński A, Bond GC. Selective hydrogenation of ethyne in ethene-rich streams on palladium catalysts, part 2: steady-state kinetics and effects of palladium particle size, carbon monoxide, and promoters. *CatalRev* 2008;50:379-469. DOI
91. Liu K, Jiang L, Huang W, et al. Atomic overlayer of permeable microporous cuprous oxide on palladium promotes hydrogenation catalysis. *Nat Commun* 2022;13:2597. DOI PubMed PMC
92. Cheng G, Jentys A, Gutiérrez OY, Liu Y, Chin Y, Lercher JA. Critical role of solvent-modulated hydrogen-binding strength in the catalytic hydrogenation of benzaldehyde on palladium. *Nat Catal* 2021;4:976-85. DOI
93. Shutt E, Winterbottom JM. Heterogeneous catalysis in the liquid phase. *Platinum Met Rev* 1971;15:94-9. DOI
94. Aramendía M, Borau V, Jiménez C, Marinas J, Sempere M, Urbano F. Optimization of the selective semi-hydrogenation of phenylacetylene with supported palladium systems. *Appl Catal* 1990;63:375-89. DOI
95. Studt F, Abild-Pedersen F, Bligaard T, Sørensen RZ, Christensen CH, Nørskov JK. Identification of non-precious metal alloy catalysts for selective hydrogenation of acetylene. *Science* 2008;320:1320-2. DOI PubMed